Biosensors and Bioelectronics 135 (2019) 111–119

Contents lists available at ScienceDirect

Biosensors and Bioelectronics

journal homepage: www.elsevier.com/locate/bios

# On-line regeneration of electrochemical biosensor for *in vivo* repetitive measurements of striatum $Cu^{2+}$ under global cerebral ischemia/reperfusion events

Hui Gu[a,*], Qi Hou[a], Yu Liu[a], Yujie Cai[a], Yanqiu Guo[a], Haoyue Xiang[b], Shu Chen[a,*]

[a] School of Chemistry and Chemical Engineering, Key Laboratory of Theoretical Organic Chemistry and Functional Molecule of Ministry of Education, Hunan University of Science and Technology, Xiangtan, Hunan 411201, PR China
[b] College of Chemistry and Chemical Engineering, Central South University, Changsha 410083, PR China

ARTICLE INFO

*Keywords:*
On-line regeneration
Copper (II) ion
Electrochemical biosensor
Repetitive measurement
Global cerebral ischemia/reperfusion

ABSTRACT

The detection of $Cu^{2+}$ ion, one of the metal ions substantial in cerebral physiology, is critical in studying brain activities and understanding brain functions. However, repetitive measurements of $Cu^{2+}$ in the progress of physiological and pathological events is still challenging, because lack of the platform for repetitive on-line detection-regeneration cycle. Herein we report the design of a regenerated electrochemical biosensor combined with the *in vivo* microdialysis system. In this biosensor, hyperbranched polyethyleneimine (hPEI) acts as a regenerated recognition unit for $Cu^{2+}$. Just by a simple rinse of ethylenediaminetetraacetic acid (EDTA) disodium salt, the $Cu^{2+}$ and $Cu^{+}$ ions on the biosensor interface were chelated with EDTA disodium salt, thus achieving the regeneration of the biosensor. In addition, 6-(ferrocenyl)hexanethiol (FcHT) serves as the inner reference moiety to elevate the sensing accuracy over regeneration cycles. As a result, this ratiometric electrochemical biosensor not only revealed high sensitivity and selectivity, but also exhibited excellent stability during multiple regeneration processing. This biosensor was capable of determining $Cu^{2+}$ with a linear range between 0.05 and 12 μM and low detection limit (LOD) of 13 nM. Then, the platform has been successfully applied in repetitive $Cu^{2+}$ analysis in rat brain under global cerebral ischemia/reperfusion events. The combination of results from 7 rats indicates global cerebral ischemia caused an obvious increase of the $Cu^{2+}$ level, while reperfusion brought this level back to normal.

## 1. Introduction

Copper (II) ion, one of the essential trace nutrient in living organisms, plays a crucial role in physiological and pathological events (Weiser and Wienrich, 1996; Luo et al., 2015). Currently, $Cu^{2+}$ serves as a critical cofactor, working with various metalloenzymes that produce cellular energy, decrease molecular oxygen, and activate signal transduction (Fife et al., 1994; Field et al., 2002). The disequilibrium of $Cu^{+}/Cu^{2+}$ can also generate reactive oxygen species (ROS), which is implicated in multiple carious neurodegenerative diseases, such as Alzheimer and Parkinson (Li et al., 1995; Bar-Or et al., 2001; Owens et al., 2011). Additionally, accumulated evidences have revealed that cerebral ischemia is one of the leading causes of mortality and neurodegenerative diseases in older population (Berenshtein et al., 1997; Fang et al., 2013; Lai et al., 2016). It is, therefore, of considerable significance to develop highly efficient approaches for cerebral $Cu^{2+}$ assay in the progress of global cerebral ischemia/reperfusion events.

Up to now, many elegant $Cu^{2+}$ determination strategies have been brought forward (Deng et al., 2013; Xianyu et al., 2013; Lin et al., 2015; Zhou et al., 2016), such as inductively coupled plasma mass spectroscopy (ICP-MS) (Becker et al., 2007), atomic emission spectrometry (ICP-AES) (Liang et al., 2006) and atomic absorption spectrometry (AAS) (Afzali et al., 2007). However, most of those methods are not suitable for the real-time measurements and *in vivo* determination. Alternatively, electrochemical methods have been considered as the prospective technique, owing to their low-cost, simplicity, and potential for real time and *in situ* detection (Rembiesa et al., 2015; Liu et al., 2017; Nocchi et al., 2017; Gu et al., 2019; Tang et al., 2019). Several practical electrochemical methods have been established on this purpose, embedding with specific recognition elements for $Cu^{2+}$ to generate corresponding electrochemical signals. Recently, Tian's group constructed several elegant electrochemical biosensors for the direct determination of $Cu^{2+}$ in ischemia model rats with high selectivity (Chai et al., 2013; Shao et al., 2013; Zhang et al., 2015). After that, a

* Corresponding authors.
*E-mail addresses:* hgu@hnust.edu.cn (H. Gu), chenshu@hnust.edu.cn (S. Chen).

https://doi.org/10.1016/j.bios.2019.03.014
Received 29 November 2018; Received in revised form 3 March 2019; Accepted 8 March 2019
Available online 09 March 2019
0956-5663/ 

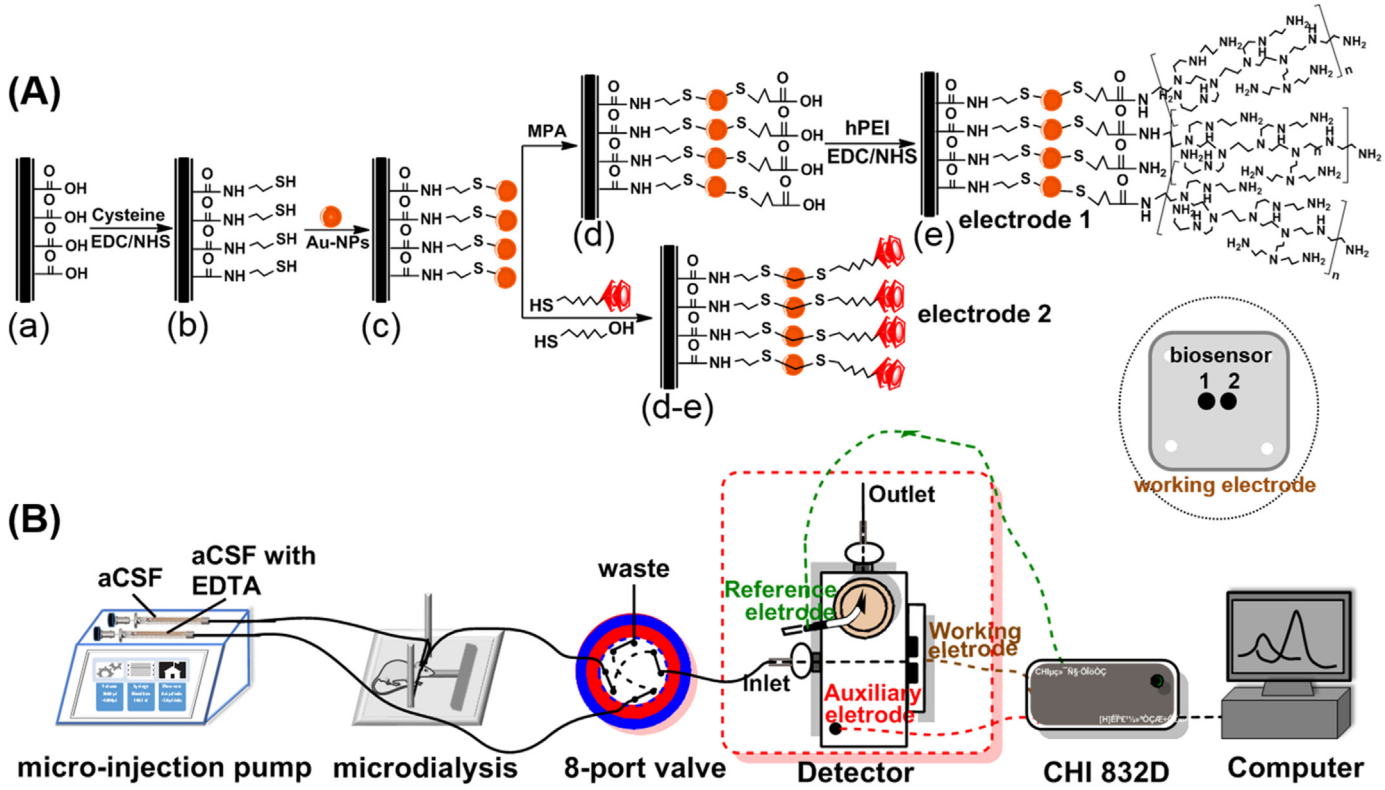


**Scheme 1.** (A) The preparation procedures for the present electrochemical biosensor; electrode 1, electrode 2: (a) activated GC, activated GC; (b) GC/Cys, GC/Cys; (c) GC/Cys/Au, GC/Cys/Au; (d) GC/Cys/Au/MPA, GC/Cys/Au/FcHT; (e) GC/Cys/Au/MPA/hPEI, GC/Cys/Au/FcHT; (B) Schematic illustration of the present *in vivo* platform for on-line regeneration of the above biosensor to repetitive measurements of cerebral $Cu^{2+}$, flowrate: 2 μL/min. The insert graph in the right of the scheme is the dual GC used for modification in A and then serves as working electrode in electrochemical detector in B.

simple electrochemical biosensor for the selective detection of $Cu^{2+}$ in AD rats was successfully built by Yu and co-authors based on the dual hydroxyl-functionalized poly (ionic liquid)-neurokinin B complex (Yu et al., 2017). Nonetheless, these disposable electrochemical sensing platforms are unable to achieve the repetitive detection of $Cu^{2+}$ in one rat under normal and pathological conditions. Therefore, the information of dynamic change of cerebral $Cu^{2+}$ level in the rats during these pathological events can be hardly acquired. In this regard, it is still of great necessity to design new regenerated electrochemical biosensors, which can fulfil the requirements for repeatedly monitoring cerebral $Cu^{2+}$ level under physiological and pathological events.

In the present work, we designed a regenerated electrochemical biosensor combined with the *in vivo* microdialysis system. On the basis of stepwise chemical reaction (Scheme 1A), hPEI was first covalently modified onto the glassy carbon (GC) electrode (electrode 1) as a regenerated recognition unit for $Cu^{2+}$. Additional 6-(ferrocenyl) hexanethiol (FcHT)-decorated electrode (electrode 2) was employed as a built-in reference moiety to elevate the sensing accuracy over regeneration cycles. The two electrodes are to construct a ratiometric electrochemical biosensor. Typically, the ratiometric strategy that involves the inner correction element and recognition unit into one electrode was limited by the total active electrode surface, and the two sections tend to disturb each other, causing the distortion of the output signals. Herein, two independent electrodes are separately cooperated into one detector (Scheme 1B, working electrode), which effectively avoided mutual interference, thus providing a more precise platform for $Cu^{2+}$ sensing. As a result, this platform was successfully validated for repetitively on-line measurement of $Cu^{2+}$ in living rat brains under the progress of global cerebral ischemia/reperfusion injury. With high robustness, reproducibility, and stability, this designed strategy is expected to offer a reliable analytical platform for repetitively on-line analysis in living systems.

## 2. Materials and methods

### 2.1. Materials and regents

Polyethylenimine (branched, hPEI, MW ~250000), 6-(ferrocenyl) hexanethiol (FcHT), 6-mercapto-1-hexanol (MCH, 97%), *N*-hydroxysuccinimide (NHS, 98%), 3-(3-dimethylaminopropyl)-1-ethylcarbodiimide hydrochloride (EDC, crystalline), uric acid (UA, 99%), and dopamine hydrochloride (DA, 99%) were purchased from Sigma-Aldrich (USA). L-asorbic acid (AA, 99.7%), $HAuCl_4{\cdot}4H_2O$ (99.9%) and all the amino acids (99%) including histidine (His), leucine (Leu), threonine (Thr), isoleucine (Ile), lysine (Lys), Cys, glutamate (Glu), valine (Val), methionine (Met), glycine (Gly), tyrosine (Tyr), tryptophan (Trp), phenylalanine (Phe), serine (Ser), arginine (Arg), were purchased from Sinopharm Chemical Reagent (China). L-cysteine (Cys, 99%), 3-mercaptopropionic acid (MPA, 99%), ethylenediaminetetraacetic acid disodium salt (EDTA disodium salt, 99%) was purchased from Admas-beta (China). Artificial cerebrospinal fluid (aCSF) was prepared by mixing NaCl (144 mM), KCl (2.7 mM), $NaH_2PO_4$ (1.75 mM), $MgCl_2$ (1 mM), $NaHCO_3$ (2.5 mM), and $CaCl_2$ (1.75 mM) solutions, then the pH value was adjusted to 7.4 with NaOH. Solution of $Ag^+$ was prepared from its nitride salt, the other solutions of metal ions were all prepared from their chloride salts with double distilled water. All the chemicals used for the experiments were of analytical grade and were used without further purification. All aqueous solutions were prepared with double distilled water.

### 2.2. Apparatus and measurements

The microstructure and morphology of the Au-NPs assembled on the glassy carbon (GC) surface were investigated by atomic force microscopy (AFM, Dimension icon PT, Bruker). X-ray photoelectron

spectroscopy (XPS) was conducted using Thermo Scientific ESCALAB 250Xi equipped with an electron flood gun and a scanning ion gun, using the AlK a radiation (1486.6 eV) as the excitation source. Electrochemical measurements were performed on an electrochemical analyzer (CHI 760e, Chenhua, China) in aCSF solution with a conventional three-electrode configuration. The working electrode is modified dual GC electrodes or single GC electrode as working electrode, the counter electrode is a Pt wire, and the reference electrode is an Ag/AgCl electrode (saturated with KCl). Differential pulse voltammetry (DPV) was conducted from 0.35 V to −0.10 V (for GC/Cys/Au/MPA/hPEI electrode) and from 0.55 V to 0 V (for GC/Cys/Au/FcHT electrode) with potential step of 4 mV, pulse width of 0.06 s, pulse period of 0.5 s and pulse amplitude of 50 mV. Electrochemical impedance spectroscopic measurements were carried out on a PGSTAT30/FRA system (Autolab, The Netherlands) in 0.1 M KCl containing 5 mM $K_3Fe(CN)_6/K_4Fe(CN)_6$, and the experimental conditions were as follows: open-circuit potential, 0.2 V; alternative voltage, 5 mV; frequency range, $0.1 - 10^5$ Hz. The equivalent circuit was obtained by the software NOVA 1.9. The real electrode surface was calculated through integration of the cathodic peak of the cyclic voltammetry (CV) from GC/Cys/Au electrodes in 0.5 M $H_2SO_4$ solution. Scan range: − 0.5–1.5 V, scan rate: 100 mV/s. The analysis of variance for cerebral $Cu^{2+}$ *in vivo* was done by the software SPSS 22.0.

### 2.3. Fabrication of the present electrochemical biosensor

The fabrication process is specifically depicted in Scheme 1A. Dual GC (3 mm diameter, CHI Company, China) electrodes were used for both off-line and on-line electrochemical experiments. Prior to surface fabrication, the GC electrodes were polished with 0.05 μm alumina powder and followed by sonication in acetone, $HNO_3$ (1:1, v/v), KOH (50%, w/w) and distilled water each for 5 min. The cleaned GC electrode were first electrochemically activated by cyclic voltammetry (CVs) scanning from − 1.0–1.0 V at a scan rate of 100 mV/s in 0.5 M $H_2SO_4$ until a stable voltammogram was obtained. Cys was then assembled onto the electrodes surface by employing EDC and NHS as catalysts to form amide between the group of –COOH at electrode surface and the $–NH_2$ moiety of Cys. The obtained electrodes functionalized by Cys on the surface with mercapto groups were referred as GC/Cys. After that, GC/Cys electrodes were immersed into the solution of as-prepared Au nanoparticles (Au-NPs, 2.33 nM) for 3 h in order to form Au-S bond, and the electrodes were referred as GC/Cys/Au. Here Au-NPs was prepared by the Classical Citrate Synthesis Method (Enustun and Turkevich, 1963) and the concentration was calculated to be 2.33 nM according to the previous report (Wang et al., 2011). Then, to prepare electrode 1, GC/Cys/Au electrode was soaked in MPA for 1 h to attach MPA through Au-S bond. This electrode containing –COOH groups at the electrode surface was referred to GC/Cys/Au/MPA. Next, hPEI was assembled onto the GC/Cys/Au/MPA surface using EDC and NHS as catalysts to form amide between –COOH groups of the MPA and the $–NH_2$ moiety of the hPEI. The final prepared electrode was denoted as GC/Cys/Au/MPA/hPEI electrode (electrode 1). To prepare electrode 2, the other obtained GC/Cys/Au electrode was immersed in 1 mM FcTH and followed in 1 mM MCH for 1 h each to attach the respect groups on the GC/Cys/Au electrode through Au-S bond. The final prepared electrode was denoted as GC/Cys/Au/FcHT electrode (electrode 2).

To confirm amplify effect of Au-NPs, GC/hPEI and Au/MPA/hPEI were prepared. GC/hPEI was prepared by assembly of hPEI onto the GC-COOH surface using EDC and NHS. To compare the accuracy of above biosensor, hPEI and FcHT were involved into one electrode to prepare GC/Cys/Au/FcHT + hPEI biosensor and GC/Cys/Au/MPA/hPEI + FcHT biosensor. Briefly, GC/Cys/Au/FcHT + hPEI electrode was obtained by stepwise linking MPA and hPEI onto GC/Cys/Au electrode as the above method. GC/Cys/Au/MPA/hPEI + FcHT electrode was constructed by modifying modify FcHT molecules onto GC /Cys/Au/MPA/hPEI electrode.

### 2.4. On-line microdialysis-electrochemical detector system

Scheme 1B shows a diagram for the on-line microdialysis-electrochemical detector system built in the lab. Microdialysis probes with minute dead volume were prepared according to the previous report. (Stamford, 1992; Zhang et al., 2013). A Pump 11 Elite programmable syringe pump (Harvard Apparatus, Holliston, USA) with a 1.0 mL gas-tight syringe delivered the blank aCSF solution into the microdialysis probe at a flowrate of 2 μL/min. An 8-port nanovolume valve equipped with two 20 μL sample loops (VICI Instruments.180 BCE, Houston, USA) was placed between the probe and electrochemical detector for the introduction of EDTA disodium salt solution. Between the detection intervals, the EDTA disodium salt solution was perfused into the detector, which took 10 min to achieve the on-line regeneration of the $Cu^{2+}$ biosensor. To minimize Taylor − Aris dispersion and other sources of dispersion, short length of 75 μm i.d. capillary tubing were used to connect each part. Connections were made with MicroTight Unions (IDEX Health & Science, Oak Harbor, USA) and 250 μm i.d. PTFE tubing (Thermo Fisher Scientific, Waltham, USA).

### 2.5. Animal experiments

All experiments involving animals were conducted with the approval of the Animal Ethics Committee in Central South University (Ethical approval number: 2017sydw029T), following previous reports (Iwasaki et al., 1989; Yanpallewar et al., 2004). Briefly, Male Sprague − Dawley rats (250 − 320 g, 6–8 weeks) Department of Laboratory Animals in Central South University, Changsha, China) were anesthetized by chloral hydrate (0.1 g/mL, initial dose of 300 mg/kg (i.p.) with additional doses of 50 mg/kg (i.p.) as required to maintain anesthesia), and then wrapped in a homeothermic blanket (69000 Series Temperature Controller, WRD Life Science, Shenzhen, China) to stabilize the body temperature at 37°C. The rat was fixed in a stereotaxic frame (WRD Life Science, Shenzhen, China) with the incisor bar set at 5 mm above the interaural line. The microdialysis probe (homemade in the lab, detailed in the supplementary experiment) was then implanted into the striatum (2.5 mm anterior of bregma, 2.5 mm lateral of midline, and 7.0 mm below dura). Two skull screws were employed to hold the probe in place by dental cement, and the scalp incision was closed with sutures. When the rats were still anesthetized, the surgeries of global cerebral ischemia/reperfusion was performed. In the opened wound through midline cervical incision, both common carotid arteries were exposed and separated from surrounding connective tissue, with special care not to break the sympathetic nerves or the vagus running close by. Global ischemia (60 min) and reperfusion (60 min) were carried out by first interdicting both carotid arteries by two hemostatic clips for ischemia and then removing the clips for reperfusion. Throughout the surgery, the rat was kept wrapped in a homeothermic blanket under anesthesia. Throughout the operation, the microdialysis probes were positioned in the striatum of rats and were perfused with a CSF solution at 2 μL/min.

### 2.6. Repetitive on-line measurements of $Cu^{2+}$ in vivo

After the tip of the probe was implanted into the striatum area, online analysis of the microdialysate was performed. The first DPV detection of $Cu^{2+}$ from normal rat was conducted when the microdialysate was delivered for 60 min for equilibration. Then, a loop of 10 mM EDTA disodium salt was loaded and injected into the detector. The $Cu^{2+}$ on the electrode surface were removed and the electrodes were recycled for the next detection. Afterwards, global ischemia (60 min) was carried out and the second DPV detection was operated. After the electrodes was again recycled by EDTA disodium salt, reperfusion (60 min) was carried out and the third DPV detection was

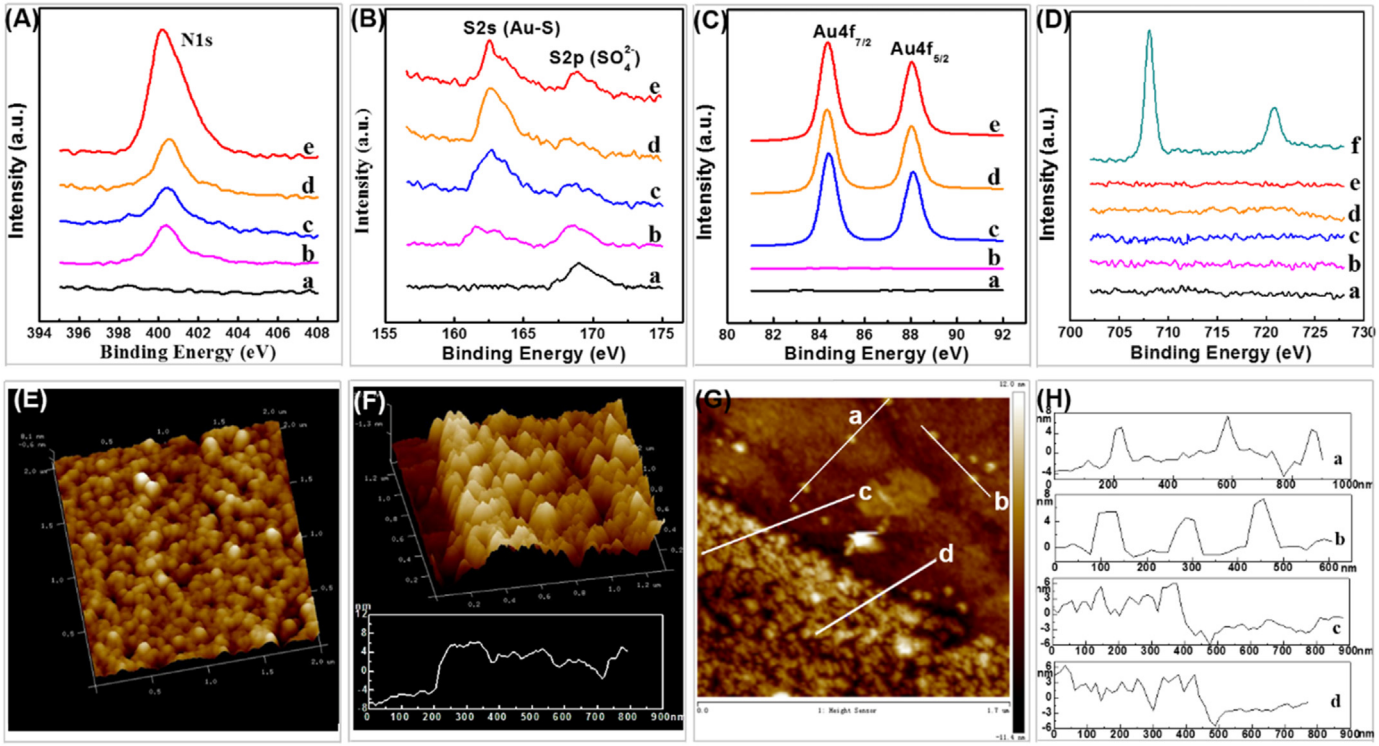


**Fig. 1.** XPS spectra of (A) N1s, (B) S2s (Au-S) and S2p ($SO_4^{2-}$), (C) $Au4f_{7/2}$ and $Au4f_{5/2}$, and (D) $Fe2p_{3/2}$ and $Fe2p_{1/2}$ for a) bare GC; b) GC/Cys; c) GC/Cys/Au; d) GC/Cys/Au/MPA; e) GC/Cys/Au/MPA/hPEI; f) GC/Cys/Au/FcHT; (E) AFM topographic image of Au-NPs assembled onto the GC/Cys surface; (F) AFM topographic image with edges for GC/Cys/Au surface; (G) AFM image of Au-NPs monolayer with ragged edges, (H) Height profiles along the line shown in G.

achieved.

## 3. Results and discussion

### 3.1. Characterization of the prepared biosensor

The process for fabrication of the biosensor illustrated in Scheme 1A was depicted as above in the Materials and Methods. Firstly, the stepwise modification of the present biosensor was tracked by XPS. As demonstrated in Fig. 1A, B (curve b), obvious N1s peak at 400.4 eV and S2s peak for sulfydryl at 162.7 eV were obtained at GC/Cys electrode, while only S2p peak for residual $SO_4^{2-}$ at 169.0 eV was obtained from bare GC (curve a), indicating the successful modification of Cys on GC electrode. After the modification of Au-NPs, clear Au 4 $f_{7/2}$ and Au 4 $f_{5/2}$ peaks at 84.4 eV and 88.0 eV (Fig. 1C, curve c) were observed, suggesting the existence of Au-NPs on the GC surface. Next, for fabrication of GC/Cys/Au/MPA/hPEI electrode, MPA was then modified on the Au surface to further covalently linking hPEI. As demonstrated in Fig. 1A, B (curve d), the intensity of N1s peak and S2s peak were

slightly strengthened due to the successful immobilization of MPA molecules on the GC/Cys/Au surface through Au − S bond. After embellished with hPEI, the intensity of N1s peak was multiplied because of the abundant amino groups in hPEI (Fig. 1A, curve e). For GC/Cys/Au/FcHT electrode, two new peaks at 708.8 and 720.6 eV for $Fe2p_{3/2}$ and $Fe2p_{1/2}$ in Fig. 1D (curve f) were observed, indicating the FcHT was favourably connected to GC/Cys/Au surface through Au − S bond.

The assembly of Au-NPs on the GC surface was also confirmed by the AFM image. As demonstrated in Fig. 1E, Au-NPs monolayer were clearly assembled on the GC surface. Furthermore, the monolayer was homogeneous, complete, and well ordered. Fig. 1F, G exhibited Au-NPs monolayer with ragged edges, on account that the solution for the electrode modification was uneven. Some monodispersed Au-NPs were observed on the bare GC area, with an average size of ~6 nm (Fig. 1H, curve a, b). And the average thickness of Au-NPs monolayer is ~6 nm (Fig. 1H, curve c, d), indicating that Au-NPs were clearly assembled on the GC surface without obvious changes in shape or size. Fig. S1 showed the CV of GC/Cys/Au electrode in 0.5 M $H_2SO_4$. A rise in anodic current at 0.24 V indicates oxide formation. Oxide reduction started at around 0.24 V in the cathodic scan. Above are the typical electrochemical performances of Au in acidic solution.

CV in 0.1 m PBS (pH 7.4) containing 1 mM $K_3[Fe(CN)_6]$ was recorded as another characterization method to further characterize the interfacial variations of the fabricated electrode at each immobilization step. As depicted in Fig. S2A, well-defined redox peaks of $[Fe(CN)_6]^{3-/4-}$ were observed at the stepwise fabrication electrodes. Prior to modification, the bare GC (curve a) was electrochemically activated in an acidic solution, thus an improved sensitivity of activated GC (curve b) was achieved. The following binding of Cys lead to an obvious decrease in the output current (curve c) because Cys molecules hindered the access of the redox probe to the electrode surface (Xian et al., 2004; Devi et al., 2013). Further immobilization of Au-NPs contributed to the enhancement of charging current (curve d), while the modification MPA molecules generated a falling current (curve e). This can be explained by the fact that the Au-NPs provide large surface area and excellent conductivity to promote the electron transfer, and the MPA molecules exert opposite effects (Shervedani and Pourbeyram, 2011). After successive modification with hPEI, the peak current increased slightly (curve f), while the peak current decreased with coordination interaction of $Cu^{2+}$ (curve g). This phenomenon may be attributed to the complex facilitate electron transfer between the abundant branched amino group in hPEI and $Fe^{3+}$ (Hirst et al., 2013). As a result, after adding $Cu^{2+}$, few active amino site is free to trap $Fe^{3+}$. To sensitively indicate the successful fabrication of the above biosensor, electrochemical impedance spectroscopy (EIS) was further employed based on the change of charge-transfer resistance ($\Delta R_{ct}$), since it was easier to define $R_{ct}$ than its redox peak currents and had little interference to the modified film. The result was shown as Nyquist plots containing a semicircular portion (Fig. S2B). The diameter of this portion was

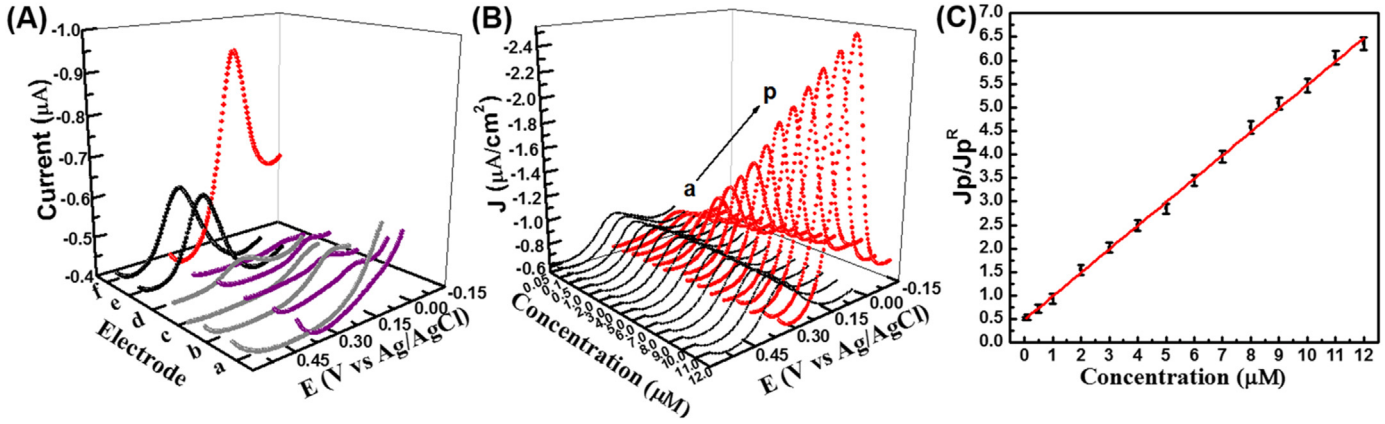


**Fig. 2.** Electrochemical behaviour of the present biosensor: (A) DPV responses in aCSF containing 4 μM $Cu^{2+}$ for electrode 1, electrode 2 in stepwised modification process, a) bare GC (purple), bare GC (gray); b) activated GC (purple), activated GC (gray); c) GC/Cys (purple), GC/Cys (gray); d) GC/Cys/Au (purple), GC/Cys/Au (gray); e) GC/Cys/Au/MPA (purple), GC/Cys/Au/FcHT (black); f) GC/Cys/Au/MPA/hPEI (red), GC/Cys/Au/FcHT (black); (B) Representative DPV responses of the present biosensor (electrode 1: GC/Cys/Au/MPA/hPEI, electrode 2: GC/Cys/Au/FcHT) in aCSF containing $Cu^{2+}$ (from a to p) of 0.05, 0.1, 0.5, 1, 2, 3, 4, 5, 6, 7, 8, 9, 10, 11, 12 μM; (C) Linear plot of $Jp/Jp^R$ results versus $Cu^{2+}$ concentrations. The error bars represent the standard deviations (SD, n = 3).

equivalent to the $R_{ct}$ and could be calculated by fitting the data using an appropriate Randles circuit (inset of Fig. S2B). The $R_{ct}$ values were as follows: bare GC (259.1 Ω, curve a), activated GC (82.1 Ω, curve b), GC/Cys (107.6 Ω, curve c), GC/Cys/Au (28.9 Ω, curve d), GC/Cys/Au/MPA (61.4 Ω, curve e), GC/Cys/Au/MPA/hPEI (151.1 Ω, curve f), GC/Cys/Au/MPA/hPEI-$Cu^{2+}$ (221.6 Ω, curve g) electrodes, respectively. These outcomes, along with the redox peak currents above indicate that the stepwise fabrication strategy to construct the present biosensor was successful.

### 3.2. Electrochemical behaviour of the biosensor

DPV was employed in the electrochemical monitoring of $Cu^{2+}$ because of its high sensitivity. Fig. 2A showed the DPV responses in aCSF containing 4 μM $Cu^{2+}$ for electrode 1, electrode 2 in stepwised modification process (curves a: bare GC, bare GC; curves b: activated GC, activated GC; curves c: GC/Cys, GC/Cys; curves d: GC/Cys/Au, GC/Cys/Au; curves e: GC/Cys/Au/MPA, GC/Cys/Au/FcHT; f) GC/Cys/Au/MPA/hPEI, GC/Cys/Au/FcHT). For electrode 1, a clear cathodic peak located at 100 mV vs Ag/AgCl was observed at the GC/Cys/Au/MPA/hPEI biosensor, while no obvious signals were obtained at other modified electrodes. This cathodic peak was ascribed to the electrochemical reduction of $Cu^{2+}$ to $Cu^{+}$. For electrode 2, another cathodic peak located at 360 mV vs Ag/AgCl was only observed at GC/Cys/Au/FcHT electrode, which is attributed to the reduction of FcHT. Consequently, the quantification of $Cu^{2+}$ in this ratiometric biosensor can be achieved based on the current ratios between the above two peaks. Such a result was also adequate to attest that the good response of the biosensor towards $Cu^{2+}$ owing to the effective combination of hPEI with $Cu^{2+}$ through coordination interaction. And the coordination reaction could be achieved in 20 min (Fig. S3).

The peak current signals between GC/Cys/Au/MPA/hPEI, GC/hPEI and Au/MPA/hPEI towards 4 μM $Cu^{2+}$ were used to compare their sensitivity regardless of the effect of surface area (Fig. S4). Obviously, the sensitivity obtained at GC/Cys/Au/MPA/hPEI electrode is ~2.5 fold greater than that at the Au/MPA/hPEI electrode, while the GC/hPEI electrode revealed negligible current response towards 4 μM $Cu^{2+}$. The assembly of Au-NPs possessed several features that improve the sensitivity of the GC/Cys/Au/MPA/hPEI eletrode: (1) the assembly of Au-NPs significant increased conductivity of the electrode (data of ESI); (2) Au-NPs exert good catalysis effect for the biosensor detection of $Cu^{2+}$; (3) the anisotropy of the assembled Au-NPs endows the biosensor an increased surface area to load more recognition unit hPEI (Mahshid et al., 2017).

The redox reactions of $Cu^{2+}$ on the GC/Cys/Au/MPA/hPEI electrode obtained at different scan rates in aCSF with 4 μM $Cu^{2+}$ (pH 7.4) were demonstrated in Fig. S5A. Both anodic and cathodic peak currents ($I_{pa}$ and $I_{pc}$) varied linearly with potential scan rate ($\nu$) in the range of 10 − 400 mV/s (Fig. S5B), suggesting the redox reaction is the surface-confined process. The peak width at half peak height ($\Delta E_{p,1/2}$) was calculated to be 76.5 ± 4.3 mV (mean ± SD, n = 3) versus Ag|AgCl at the scan rate of 100 mV/s. According to Laviron's equation (Laviron, 1979), the kinetics of heterogeneous electrontransfer rate constant ($k_{et}$) was estimated to be 2.08 ± 0.06 $s^{-1}$.

To assess the sensitivity of the designed electrochemical biosensor, DPV responses at this biosensor towards standard $Cu^{2+}$ with different concentrations were measured. As illustrated in Fig. 2B, the reduction peak located at 100 mV increased with the increasing of $Cu^{2+}$ concentrations, while the reduction peak located at 360 mV stayed almost constant, resulting in the ratiometric measurement of $Cu^{2+}$. The current density of this reduction peak ($Jp^R$) stayed almost constant, while the current density of the reduction peak at 100 mV (Jp) increased with the increasing concentrations of $Cu^{2+}$. The current densities ratio between the two peaks was used to quantify of $Cu^{2+}$, in which the current density at 100 mV for $Cu^{2+}$ was denoted as Jp, and $Ip^R$ represented the current density of FcHT at 360 mV. This ratio ($Jp/Jp^R$) exhibited a good linearity with the concentration of $Cu^{2+}$ ranging from 0.05 μM to 12 μM, with a sensitivity of 153.4 mA/($cm^{-2}$·M). The detection limit (LOD) was 13 nM estimated from 3σ of the baseline signals. This LOD value is equal to or superior to that of previously reported $Cu^{2+}$ detection platforms, which indicates that the present electrochemical biosensor holds great promising for $Cu^{2+}$ assay in a biological system (Chai et al., 2013; Shao et al., 2013; Yuan et al., 2014; Hu et al., 2015; Luo et al., 2015; Zhang et al., 2015; Sun et al., 2016; Ma et al., 2017; Yu et al., 2017; Wu et al., 2018). A table has been summarized to more clearly compare our method with other published strategies (Table S1).

Meanwhile, in order to check the accuracy of the biosensor that involves the inner correction element and recognition unit into one electrode, GC/Cys/Au/FcHT + hPEI electrode and GC/Cys/Au/MPA/hPEI + FcHT electrode were prepared. As demonstrated in Fig. S6, for GC/Cys/Au/FcHT + hPEI electrode (curve a), the peak current density of FcHT remained stable, while the signal of $Cu^{2+}$ decreased drastically. For GC/Cys/Au/MPA/hPEI + FcHT electrode (curve c), the signal of $Cu^{2+}$ kept pace with the present biosensor (curve b), while the current response of FcHT dropped dramatically. A reasonable explanation might be that the limited active biding sites of Au-NPs disturbed the modified molecule number of FcHT and hPEI, leading to

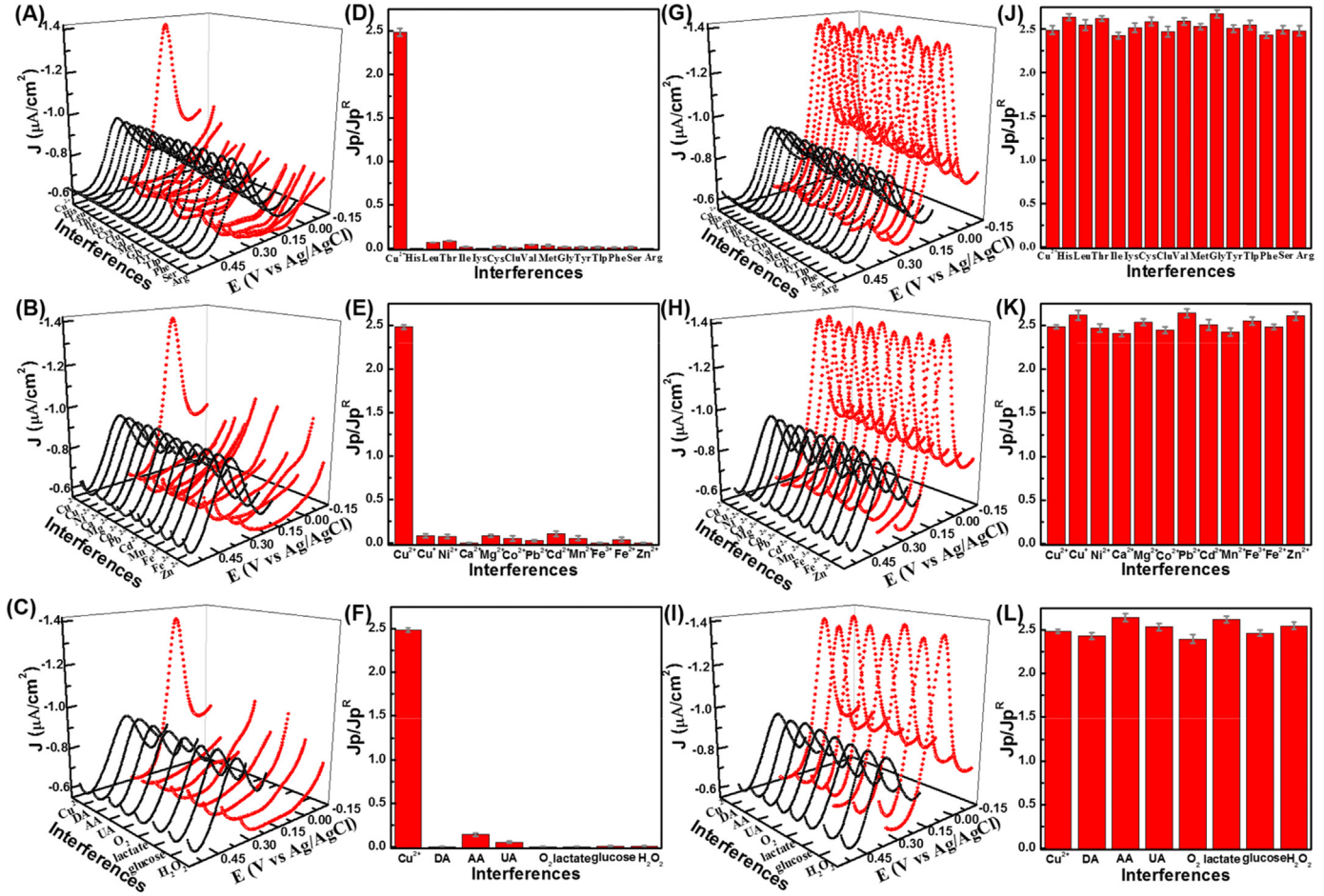


**Fig. 3.** DPV responses of the present biosensor towards $Cu^{2+}$ (4 μM) or different interference, (A) amino acid: His, Leu, Thr, Ile, Lys, Cys, Glu, Val, Met, Gly, Tyr, Trp, Phe, Ser, Arg (2 μM for His, Glu, 10 μM for others); (B) other metal ions: $Ni^{2+}$, $Ca^{2+}$, $Mg^{2+}$, $Co^{2+}$, $Pb^{2+}$, $Cd^{2+}$, $Mn^{2+}$, $Fe^{3+}$, $Fe^{2+}$, $Zn^{2+}$ (1 mM for $Ca^{2+}$, $Mg^{2+}$, 10 μM for others); (C) typical biological species: DA (10 μM), AA (100 μM), UA (10 μM), $O_2$ (0.25 mM), lactate (1 mM), glucose (1 mM), $H_2O_2$ (1 μM). Selectivity investigations of $Jp/Jp^R$ results versus $Cu^{2+}$ or (D) amino acid, (E) other metal ions, (F) typical biological species, (mean ± SD, n = 3). DPV responses of the present biosensor towards $Cu^{2+}$ (4 μM) containing different interference (G) amino acid, (H) other metal ions, (I) typical biological species, the concentrations are the same with above. Competition tests of $Jp/Jp^R$ results versus $Cu^{2+}$ containing (J) amino acid, (K) other metal ions, (L) typical biological species. The error bars represent the SD (SD, n = 3).

abnormal output signals of FcHT and $Cu^{2+}$. The present method separately established two independent electrodes, which effectively avoided mutual interference, thus providing a more precise platform for $Cu^{2+}$ sensing.

### 3.3. Selectivity, stability, and reproducibility

The complexity of cerebral microdialysate presents a great challenge to the electrochemical biosensor for $Cu^{2+}$ detection not only in the sensitivity, but also more particularly in selectivity. The selectivity of the present method was evaluated by monitoring the $Jp/Jp^R$ values of the biosensor to sense the potential interferences in the absence/presence of $Cu^{2+}$. The possible interferences for $Cu^{2+}$ detection that commonly coexist in cerebral systems were other metal ions ($Cu^{+}$, $Ni^{2+}$, $Ca^{2+}$, $Mg^{2+}$, $Co^{2+}$, $Pb^{2+}$, $Cd^{2+}$, $Mn^{2+}$, $Fe^{3+}$, $Fe^{2+}$, $Zn^{2+}$), amino acids (His, Leu, Thr, Ile, Lys, Cys, Glu, Val, Met, Gly, Tyr, Trp, Phe, Ser, Arg) and several typical biological species (DA, AA, UA, $O_2$, lactate, glucose, $H_2O_2$). Remarkably, as shown in Fig. 3A, B, C, no obvious electrochemical responses were observed at 100 mV with additions of these mentioned interferences, which can be evaluated from the dramatic decrease in the $Jp/Jp^R$ ratios compared with that of $Cu^{2+}$ (Fig. 3D, E, F). Furthermore, for the competition test, all the above potential interferences showed negligible effects on the current signal for $Cu^{2+}$ sensing (Fig. 3G, H, I), which was also revealed by the almost unaltered $Jp/Jp^R$ ratios (Fig. 3J, K, L). All these evidences indicate the high selectivity of the present biosensor for $Cu^{2+}$ determination against other metal ions, amino acids and biological species in the cerebral fluids, which is attributed to the strong coordination between hPEI and $Cu^{2+}$.

The stability of the modified molecule layers on GC electrodes was also studied. As shown in Fig. S7A, no obvious signal decrease was observed on these six biosensor for detection of 4 μM $Cu^{2+}$ over 6 days. Furthermore, in consideration of the existence of biosensor-to-biosensor variance applied on different rats, the inter assay precision of six separately fabricated biosensors was examined by their DPV responses in aCSF solution with 4 μM $Cu^{2+}$. As demonstrated in Fig. S7B, The RSD of these six measurements was 6.83%, which demonstrates the stepwise strategy for constructing $Cu^{2+}$ electrochemical biosensor with good precision and acceptable fabrication repeatability.

### 3.4. EDTA disodium salt-mediated on-line regeneration

On-line regeneration of the present biosensor has been investigated before the *in vivo* experiments. First of all, 6 successive measurement from one ratiometric biosensor without regeneration by EDTA disodium salt contributed to consecutive signal decreasing (Fig. 4A, C). The RSD of these determinations was 17.27%. Then, on-line regeneration of the present biosensor combined with the *in vivo* microdialysis system has

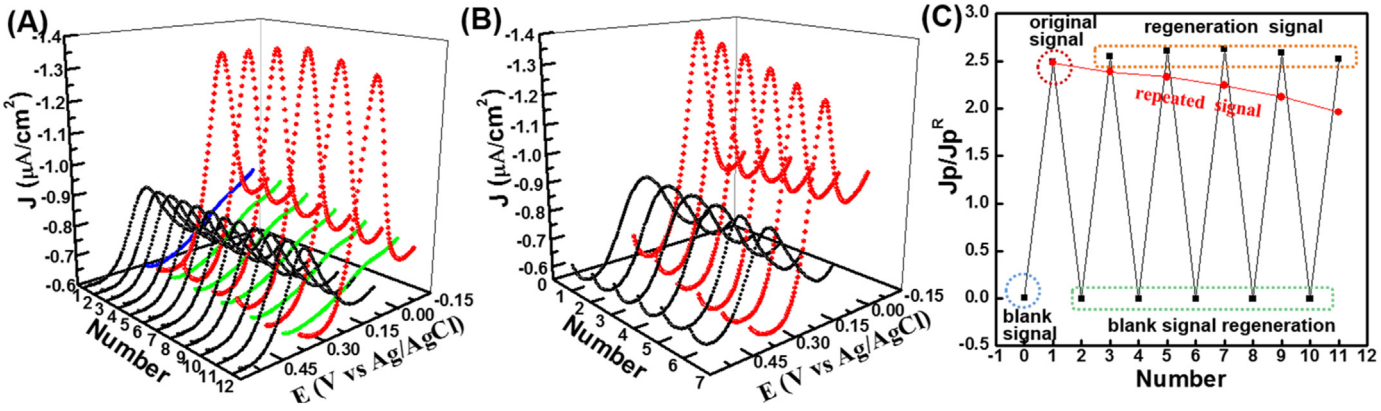


**Fig. 4.** EDTA disodium salt-mediated on-line regeneration: (A) Repeated DPVs obtained at the prepared biosensor in aCSF solution containing 4 μM $Cu^{2+}$, GC/Cys/Au/MPA/hPEI electrode: red curve, GC/Cys/Au/FcHT electrode: black curve; (B) DPVs of 5 detection-regeneration cycles obtained at the prepared biosensor in the on-line EDTA disodium salt -mediated regeneration process, GC/Cys/Au/MPA/hPEI electrode: blue curve for blank signal, red curves for original signal and regeneration signal, green curves for blank signal of regeneration, GC/Cys/Au/FcHT electrode: black curve; (C) Summary of the $Jp/Jp^R$ results from A and B.

been studied. The first DPV response of the ratiometric biosensor in blank aCSF solution was recorded as the blank signal. Then, the second DPV response was recorded as the original signal after the biosensor was incubated with the aCSF solution containing 4 μM $Cu^{2+}$ for 20 min. And then, a loop (20 μL) of 10 mM EDTA disodium salt was loaded and injected into the detector, which took 10 min to finish the on-line regeneration of the $Cu^{2+}$ biosensor. In this process, $Cu^{2+}$ and $Cu^{+}$ ions on the biosensor interface was removed by EDTA disodium salt, forming the second DPV response as the blank signal of regeneration. EDTA disodium salt exerts a higher affinity for binding $Cu^{2+}$ and $Cu^{+}$ ions than hPEI. With EDTA disodium salt passed on the biosensor, $Cu^{2+}$ and $Cu^{+}$ ions prefer binding to EDTA disodium salt and left from biosensor surface (Juang and Yan, 2001; Maketon et al., 2008; Maketon and Ogden, 2008). This process was denoted as one detection-regeneration cycle, and the minimal interval for one cycle was 30 min. Afterwards, when the biosensor was incubated with the aCSF solution containing 4 μM $Cu^{2+}$, the $Cu^{2+}$ was relinked with hPEI to rebuild the biosensor, generating the corresponding DPV response as the regeneration signal. This regeneration process was repeated 5 times for one ratiometric biosensor (Fig. 4B, C). The relative standard deviation (RSD) of these determinations was only 6.20%, indicating that this ratiometric biosensor has a benign regeneration ability for $Cu^{2+}$ monitoring. Therefore, an explicit conclusion can be drawn that the regeneration process is an indispensable procedure to insure stable signals for repetitive $Cu^{2+}$ assay. The relative consistency of the original signal and regeneration signals initially capacitate this prepared biosensor to repeatedly detection of $Cu^{2+}$ over regeneration cycles.

In addition, long-term stability of regeneration was investigated. The present biosensor was repeated 3 detection-regeneration cycles every day, stored in darkness for a week at 4°C. 89.4% of its original signal was retained, illustrating the fabricated biosensor possesses reliable long-term stability over detection-regeneration cycles.

### *3.5. Repetitively on-line measurements of $Cu^{2+}$ in rat brain in the progress of global cerebral ischemia/reperfusion events*

As demonstrated above, the developed electrochemical biosensor for $Cu^{2+}$ showed high sensitivity and selectivity, as well as good regeneration ability, which provided a reliable platform for repetitively on-line measurements of cerebral $Cu^{2+}$. After continuous perfusion of microdialyte from normal rat for 60 min, the first DPV detection of $Cu^{2+}$ from normal rat was conducted (Fig. 5A, B, C, D, E, F, G). The basal level of $Cu^{2+}$ (1.65 ± 0.23 μM, mean ± SEM, n = 6) from the brain microdialysates was summarized in Table S2, which are close to the reported values (Chai et al., 2013; Yu et al., 2017). Furthermore, after global cerebral ischemia injury was performed for 60 min, the peak current remarkably increased. By then the concentration of $Cu^{2+}$ was 5.14 ± 0.63 μM (mean ± SEM, n = 6) ($p < 0.01$), 3.12 fold greater than the basal level. The results are largely in agreement with previous reports, but slightly lower than these reports, possibly due to the ischemia model rats built by different ways (Ma et al., 1999; Shao et al., 2013; Zhang et al., 2015). After removing the clips to reperfusion, the $Cu^{2+}$ concentration almost declined to the basal level 1.71 ± 0.21 μM (mean ± SEM, n = 6) ($p > 0.05$) in 60 min. The results of one-way ANOVA (normal-ischemia and normal-reperfusion) indicate that there were no significant differences in $Cu^{2+}$ levels of the rats under normal and reperfusion condition, while 60 min global cerebral ischemia injury exerted a significant effect on the cerebral $Cu^{2+}$ level. The intracellular level of $Cu^{2+}$ plays a prominent role to mediate the reactive oxygen-derived active species in tissue injury (Ambrosio et al., 1987; Lesnefski, 1992). It has been reported that the release of $Cu^{2+}$ was the results of oxidative stress response of cells and tissues to deal with injury following global cerebral ischemia event (> 35 min) (Chevion et al., 1993; Berenshtein et al., 1997). The potential source of the released $Cu^{2+}$ is the catabolism of copper-containing protein including cytochrome oxidase, lysyl oxidase and diamine oxidase (Berenshtein et al., 1997). Such catabolism is a normal consequence of the dismantling of the respiratory apparatus during global cerebral ischemia process (Eaton, 1996). Following 60 min of reperfusion the intracellular level of $Cu^{2+}$ in rat brain decreased to basal level. The cell and tissue are gradually recovered from the injury (Voogd et al., 1994).

## 4. Conclusion

In summary, we have fabricated an on-line regenerated electrochemical biosensor combined with the *in vivo* microdialysis, which demonstrated high sensitivity, selectivity, and stability towards $Cu^{2+}$ sensing over multiple regeneration cycles. This reliable platform have been successfully applied in repetitive determination of cerebral $Cu^{2+}$ ion levels in the progress of global cerebral ischemia/reperfusion events. As a result, $Cu^{2+}$ level increased obviously among global cerebral ischemia injury, while returned to normal with reperfusion. Therefore, the $Cu^{2+}$ level could be regarded as an important indicator of global cerebral ischemia, which may act as a potential biomarker to diagnose early neurodegenerative diseases. The present study not only provides a good strategy to construct regenerated and stable electrochemical biosensors based on macromolecule for specific determination of metal ions, but also establishes a reliable on-line analytical platform for *in vivo* monitoring important biomarkers repetitively. Meanwhile, this work might pave the way for on-line monitoring the significant species in the progress of physiological and pathological events, which might boost the chance to understand the mechanism of these

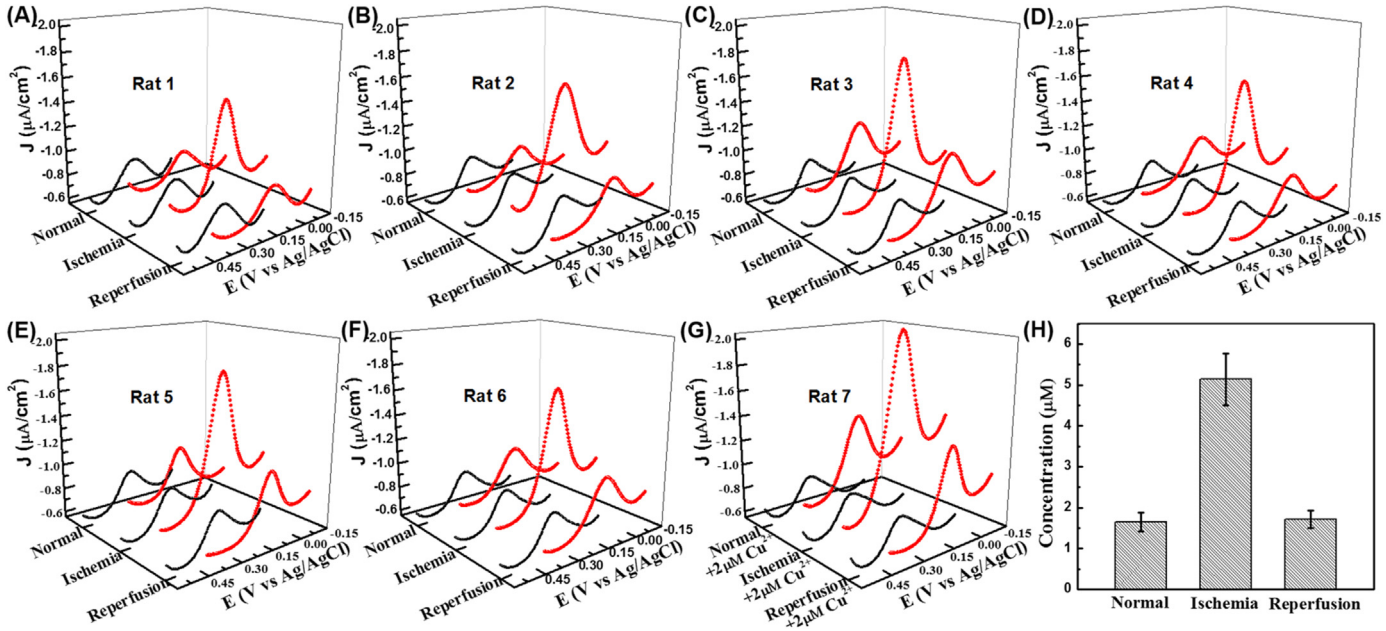


**Fig. 5.** On-line DPV responses obtained at the present biosensor for the rat brain in the progress of cerebral ischemia/reperfusion event. Perfusion solution for microdialysis: (A)-(F) aCSF; (G) aCSF with 2 μM $Cu^{2+}$; (H) Concentrations of $Cu^{2+}$ in rats 1–6 under normal, ischemia and reperfusion condition, data are expressed as mean ± standard error of mean (SEM, n = 6). Furthermore, to verify the accuracy of the $Cu^{2+}$ determined by the present biosensor, we adopted aCSF with standard 2 μM $Cu^{2+}$ to collect microdialysate for on-line analysis. According to the obtained DPV signals (Fig. 5G), the $Cu^{2+}$ quantitative concentrations was calculated and presented in Table S2. Compared with the results of microdialysate collected form blank aCSF, increased $Cu^{2+}$ concentrations at both basal level and pathological level were obtained. However, it is worth noting that, to draw a clear conclusion of the recovery rate of the added standard $Cu^{2+}$ is hard. This is because the diffusion of $Cu^{2+}$ ions between the perfusate in the probe and cerebrally extracellular fluid is complicated to acquire a quantitative data. Nonetheless, this comparison implies that the developed regenerated biosensor coupled with microdialysis system provides a relatively reliable approach for on-line determining $Cu^{2+}$ ions *in vivo*.

physiological and pathological processes. Nonetheless, the widespread clinical application of the present on-line system to monitor $Cu^{2+}$ in human brain remains technical hurdles. The measurements are interrupted by regeneration processes and the minimal interval between 2 measurements is 30 min, which enables the present approach hardly achieving real-time monitoring. Exploitation in biosensors with the ability to realize continuous real-time determination of $Cu^{2+}$ is extremely promising for elevating the potential of its clinical practice.

## CRediT authorship contribution statement

**Hui Gu:** Conceptualization, Data curation, Formal analysis, Funding acquisition, Investigation, Methodology, Project administration, Resources, Software, Supervision, Validation, Visualization, Writing - original draft, Writing - review & editing. **Qi Hou:** Data curation, Investigation, Software. **Yu Liu:** Data curation, Investigation. **Yujie Cai:** Data curation, Investigation. **Yanqiu Guo:** Data curation, Investigation. **Haoyue Xiang:** Methodology, Resources. **Shu Chen:** Funding acquisition, Methodology, Project administration, Resources, Supervision, Validation, Visualization, Writing - review & editing.

## Acknowledgements

This work was supported by the National Natural Science Foundation of China (Project No. 21605047), Natural Science Foundation of Hunan Provincial (Project No. 2017JJ3080 and 2019JJ60005), and Science and Technology Planning Project of Hunan Province (Project No. 17C0627).

## Declarations of interest

None.

## Appendix A. Supplementary material

Supplementary data associated with this article can be found in the online version at doi:10.1016/j.bios.2019.03.014.

## References

Afzali, D., Mostafavi, A., Taher, M.A., Moradian, A., 2007. Talanta 71, 971–975.
Ambrosio, G., Zweier, J.L., Jacobus, W.E., Weisfeldt, M.L., Flaherty, J.T., 1987. Arch. Biochem. Biophys. 315, 235–243.
Bar-Or, D., Rael, L.T., Lau, E.P., Rao, N.K., Thomas, G.W., Winkler, J.V., Yukl, R.L., Kingston, R.G., Curtis, C.G., 2001. Biochem. Biophys. Res. Commun. 284, 856–862.
Becker, J.S., Matusch, A.C., Dobrowolska, D.J., Zoriy, M.V., 2007. Anal. Chem. 79, 6074–6080.
Berenshtein, E., Mayer, B., Goldberg, C., Kitrossky, N., Chevion, M., 1997. J. Mol. Cell Cardiol. 29, 3025–3034.
Chai, X., Zhou, X., Zhu, A., Zhang, L., Qin, Y., Shi, G., Tian, Y., 2013. Angew. Chem. Int. Ed. 52, 8129–8133.
Chevion, M., Jiang, Y., Har-El, R., Berenshtein, E., Uretzky, G., Kitrossky, N., 1993. Proc. Natl. Acad. Sci. USA 90, 27–37.
Deng, J., Yu, P., Yang, L., Mao, L., 2013. Anal. Chem. 85, 2516–2522.
Devi, R., Batra, B., Lata, S., Yadav, S., Pundir, C.S., 2013. Process Biochem. 48, 242–249.
Eaton, J.W., 1996. Redox Rep. 2, 215.
Enustun, B.V., Turkevich, J., 1963. J. Am. Chem. Soc. 85, 3317.
Fang, K.M., Cheng, F.C., Huang, Y.L., Chung, S.Y., Jian, Z.Y., Lin, M.C., 2013. Biol. Trace Ele. Res 152, 66–74.
Field, L.S., Luk, E., Culotta, V.C., 2002. J. Bioenerg. Biomembr. 34, 373–379.
Fife, R.S., Moody, S., Houser, D., Proctor, C., 1994. Biochim. Biophys. Acta 1201, 19–22.
Gu, H., Liu, Y., Ren, T., Xia, W., Guo, Y., Shi, G., 2019. Sens. Actuators B Chem. 287, 356–363.
Hu, R., Gou, H., Mo, Z., Wei, X., Wang, Y., 2015. Ionics 21, 3125–3133.
Iwasaki, Y., Ito, S., Suzuki, M., Nagahori, T., Yamamoto, T., Konno, H., 1989. J. Neurol. Sci. 90, 155–165.
Juang, R.S., Yan, G.S., 2001. J. Membr. Sci. 186, 53–61.
Lai, M., Wang, D., Lin, Z., Zhang, Y., 2016. J. Stroke Cerebrovasc. Dis. 25, 214–219.
Laviron, E., 1979. J. Electroanal. Chem. 101, 19–28.
Lesnefski, E.J., 1992. Free Radic. Biol. Med. 12, 429–446.
Li, Y., Kuppusamy, P., Zweier, J.L., Trush, M.A., 1995. Chem. Biol. Interact. 94, 101–120.
Liang, P., Cao, J., Liu, R., Liu, Y., 2006. Microchim. Acta 159, 35–40.
Lin, Y., Wang, C., Li, L., Wang, H., Liu, K., Wang, K., Li, B., 2015. ACS Appl. Mater. Inter 7, 27262–27270.

Liu, W., Dong, H., Zhang, L., Tian, Y., 2017. Angew. Chem. Int. Ed. 56, 16328–16332.
Luo, Y., Zhang, L., Liu, W., Yu, Y., Tian, Y., 2015. Angew. Chem. Int. Ed. 54, 14053–14056.
Ma, H., Wang, Z., Zeng, Y., Han, H., Liu, G., 1999. Chin. Chem. Lett. 10, 243–246.
Ma, S., Zhou, Q.Y., Mu, F.Y., Chen, Z.H., Ding, X.Y., Zhang, M., Shi, G., 2017. Analyst 142, 3341–3345.
Mahshid, S.S., Vallée-Bélisle, A., Kelley, S.O., 2017. Anal. Chem. 89, 9751–9757.
Maketon, W., Zenner, C.Z., Ogden, K.L., 2008. Environ. Sci. Technol. 42, 2124–2129.
Maketon, W.K., Ogden, K.L., 2008. IEEE T-SEM 21, 481–485.
Nocchi, S., Bjorklund, S., Svensson, B., Engblom, J., Ruzgas, T., 2017. Biosens. Bioelectron. 93, 9–13.
Owens, S.E., Summar, M.L., Ryckman, K.K., Haines, J.L., Reiss, S., Summar, S.R., Aschner, M., 2011. Neurotoxicology 32, 769–775.
Rembiesa, J., Gari, H., Engblom, J., Ruzgas, T., 2015. Int. J. Pharm. 496, 636–643.
Shao, X., Gu, H., Wang, Z., Chai, X., Tian, Y., Shi, G., 2013. Anal. Chem. 85, 418–425.
Shervedani, R.K., Pourbeyram, S., 2011. Sens. Actuat. B-Chem. 160, 145–153.
Hirst, N.A., Hazelwood, L.D., Jayne, D.G., Millner, P.A., 2013. Sens. Actuat. B-Chem 186, 674–680.
Stamford, J.A., 1992. Monitoring Neuronal Activity. Oxford University Press, Oxford, pp. 149–155.
Sun, X., Cai, C., Liu, T., Zhang, G., Cai, D., Xiong, S., Wu, Z., 2016. Anal. Meth 8, 303–310.
Tang, H., Cai, D., Ren, T., Xiong, P., Liu, Y., Gu, H., Shi, G., 2019. Anal. Biochem 567, 63–71.
Voogd, A., Sluiter, W., Koster, J.E., 1994. Free Radic. Biol. Med. 16, 453–458.
Wang, C.M., Chung, S.Y., Jao, H.J., Hung, W.H.S., 2011. J. Phys. Chem. C. 115 (5), 1978–1984.
Weiser, T., Wienrich, M., 1996. Brain Res. 742, 211–218.
Wu, X., Wu, L., Cao, X., Li, Y., Liu, A., Liu, S., 2018. RSC Adv. 8, 20000–20006.
Xian, Y., Wang, H., Zhou, Y., Pan, D., Liu, F., Jin, L., 2004. Electrochem. Comm. 6, 1270–1275.
Xianyu, Y., Zhu, K., Chen, W., Wang, X., Zhao, H., Sun, J., Wang, Z., Jiang, X., 2013. Anal. Chem. 85, 7029–7032.
Yanpallewar, S.U., Rai, S., Kumar, M., Acharya, S.B., 2004. Pharmacol. Biochem. Behav. 79, 155–164.
Yu, Y., Yu, C., Yin, T., Ou, S., Sun, X., Wen, X., Zhang, L., Tang, D., Yin, X., 2017. Biosens. Bioelectron. 87, 278–284.
Yuan, Z., Cai, N., Du, Y., He, Y., Yeung, E.S., 2014. Anal. Chem. 86, 419–426.
Zhang, J., Jaquins-Gerstl, A., Nesbitt, K.M., Rutan, S.C., Michael, A.C., Weber, S.G., 2013. Anal. Chem. 85, 9889–9897.
Zhang, L., Han, Y., Zhao, F., Shi, G., Tian, Y., 2015. Anal. Chem. 87, 2931–2936.
Zhou, Q., Lin, Y., Xu, M., Gao, Z., Yang, H., Tang, D., 2016. Anal. Chem. 88, 8886–8892.